

Supporting Information

## Reverse Slipping Strategy for Bulk-Reduced $\text{TiO}_{2-x}$

### Preparation from Magnéli Phase $\text{Ti}_4\text{O}_7$

**Figure S1** Structure correspondence between Rutile phase  $\text{TiO}_2$  and Magnéli phase  $\text{Ti}_4\text{O}_7$ .

**Table S1** The corresponding Miller indices between  $\text{Ti}_4\text{O}_7$  and Rutile  $\text{TiO}_2$ .

**Figure S2** XRD result of the reheated sample.

**Figure S3** XRD result of the contrast sample using Ti powder as the precursor.

**Figure S4** The live FFT results using Digital Micrograph software.

**Figure S5** The structure models for (a)  $\text{Ti}_4\text{O}_7$  at  $[1\ 0\ 0]_{\text{T}}$  and (d) rutile  $\text{TiO}_2$  at  $[-1\ 0\ 1]_{\text{R}}$ .

**Table S2** The information of  $d$ -spacing and angle for the base vectors.

**Figure S6** TEM of the planar defects in the products.

**Table S3** The loss of oxygen in products  $\text{TiO}_{2-x}$  was calculated with TG results.

**Figure S7** The TG results of the products.

**Figure S8** Digital photo and  $E_g$  of the supplementary experiment.

**Figure S9** UV-visible diffuse reflection spectrum (DRS) of the as-prepared mixtures.

**Figure S10** General photo-thermal response curve obtained in this work.

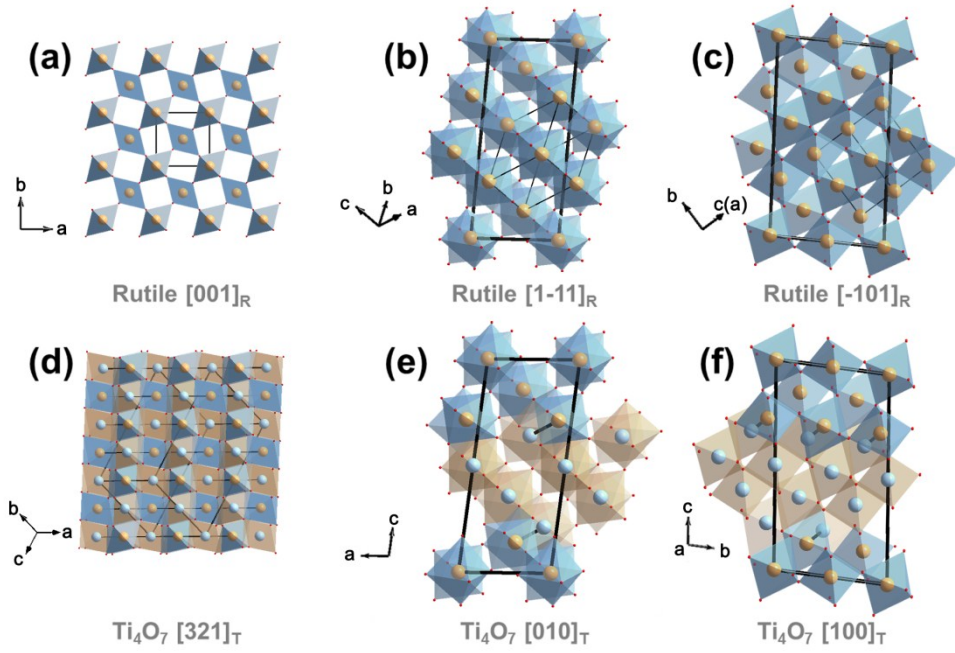


**Figure S1** Structural correspondence between Rutile phase  $\text{TiO}_2$  (a-c) and Magnéli phase  $\text{Ti}_4\text{O}_7$  (d-f). Triclinic coordinate system of  $\text{Ti}_4\text{O}_7$  was added in rutile structure (b-c). (a) Octahedral structure of  $[001]_R$  orientation, in which the footnote ‘R’ means Rutile phase  $\text{TiO}_2$ . (b) Octahedral structure of  $[1\bar{1}1]_R$  orientation, where  $a_T = -a_R + c_R$ . (c) Octahedral structure of  $[\bar{1}01]_R$  orientation, where  $b_T = a_R - b_R + c_R$ . (d) Octahedral structure of  $[3\bar{2}\bar{1}]_T$  orientation, in which the footnote ‘T’ means Magnéli phase  $\text{Ti}_4\text{O}_7$ . (e-f) The slipping parts were colored in orange. In this work, the structural models were downloaded from ICSD database (icsd#6098 for  $\text{Ti}_4\text{O}_7$ , icsd#88625 for rutile  $\text{TiO}_2$ ) and the coordinate changes refer to the work of Andersson, et al.<sup>1,2</sup>

**Table S1** The corresponding Miller indices between  $\text{Ti}_4\text{O}_7$  and Rutile  $\text{TiO}_2$ .

Miller Indices of $\text{Ti}_4\text{O}_7$	Miller Indices of $\text{TiO}_2$	Miller Indices of $\text{Ti}_4\text{O}_7$	Miller Indices of $\text{TiO}_2$	
$[3\bar{2}1]_T$	$\leftrightarrow$	$7[001]_R$	$\leftrightarrow$	$(110)_R$
$[100]_T$	$\leftrightarrow$	$-[10\bar{1}]_R$	$\leftrightarrow$	$(101)_R$
$[010]_T$	$\leftrightarrow$	$[1\bar{1}1]_R$	$\leftrightarrow$	$(200)_R$
$[001]_T$	$\leftrightarrow$	$[122]_R$	$\leftrightarrow$	$(111)_R$
$[4\bar{2}\bar{1}]_T$	$\leftrightarrow$	$-7[100]_R$	$\leftrightarrow$	$(210)_R$
$(024)_T$	$\leftrightarrow$	$2/7(414)_R$	$\leftrightarrow$	$(211)_R$
$(008)_T$	$\leftrightarrow$	$8/7(121)_R$	$\leftrightarrow$	$(002)_R$
$(0\bar{2}4)_T$	$\leftrightarrow$	$(020)_R$	$\leftrightarrow$	$(310)_R$
$(0\bar{2}2)_T$	$\leftrightarrow$	$-2/7(1\bar{5}1)_R$	$\leftrightarrow$	$(221)_R$
$2/3(013)_T$	$\leftrightarrow$	$2/21(535)_R$	$\leftrightarrow$	$(301)_R$
$2/3(023)_T$	$\leftrightarrow$	$2/3(101)_R$	$\leftrightarrow$	$(127)_R$
$(\bar{1}02)_T$	$\leftrightarrow$	$1/7(65\bar{1})_R$	$\leftrightarrow$	$-(2\bar{3}\bar{7})_T$
$(104)_T$	$\leftrightarrow$	$(011)_R$	$\leftrightarrow$	$-(3\bar{1}\bar{7})_T$
			$\leftrightarrow$	$(038)_T$
			$\leftrightarrow$	$(212)_R$

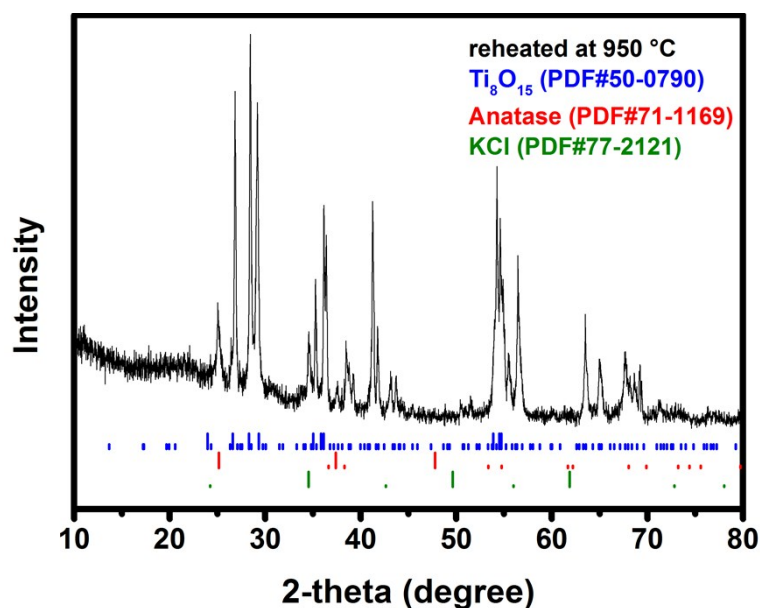


**Figure S2** XRD result of the reheated sample (15 mol%  $\text{KClO}_4$ , 950 °C, 2h). The main phase in the as-prepared sample was  $\text{Ti}_8\text{O}_{15}$ , the others were  $\text{TiO}_2$  and impurity product KCl. Rutile phase disappeared when reheated, and the more complex Magnéli phase  $\text{Ti}_8\text{O}_{15}$  became the main composition. It seemed that the latter ordered structure required a certain temperature to slip and rearrange.

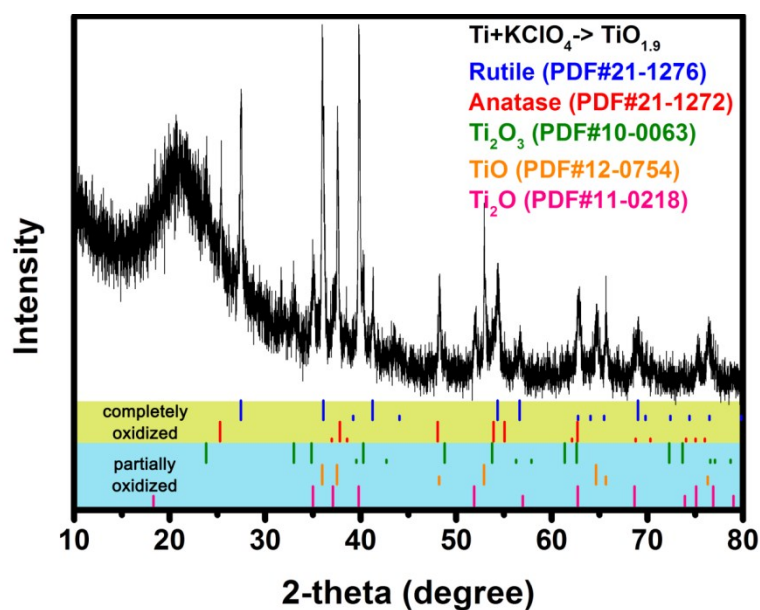


**Figure S3** XRD result of the contrast sample ( $\text{Ti} + \text{KClO}_4 \rightarrow \text{TiO}_{1.9}$ , 600 °C, 2h). There are two problems in using Ti as raw material. One is that the particles size will affect the oxidation degree, and the other is the mixing phase of rutile and anatase  $\text{TiO}_2$ , which disappear in the experimental of  $\text{Ti}_4\text{O}_7$  as raw material. **It indicates that slip strategy in this work improves the selectivity of product phase structure.**

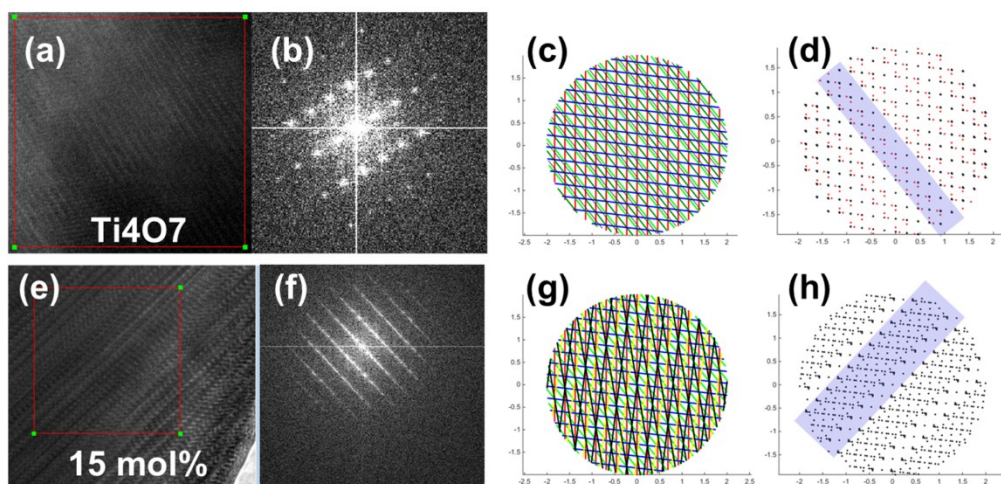


**Figure S4** The live FFT results using DigitalMicrograph software ( $\text{Ti}_4\text{O}_7$ : a,b; 15 mol% products: e,f) from real space to reciprocal space and the simulated calculation results based on diffraction points (Figure 3c, 3f) from reciprocal space to real space ( $\text{Ti}_4\text{O}_7$ : c, d; 15 mol% products: g, h). The formula of simulation calculation is based on such a theory: the vector for each point in reciprocal space corresponds to a crystal plane in real space. The direction of vector is the normal direction of the plane, and the size of vector is the reciprocal of the plane spacing. The above analysis results also showed that the calibration results were reasonable.

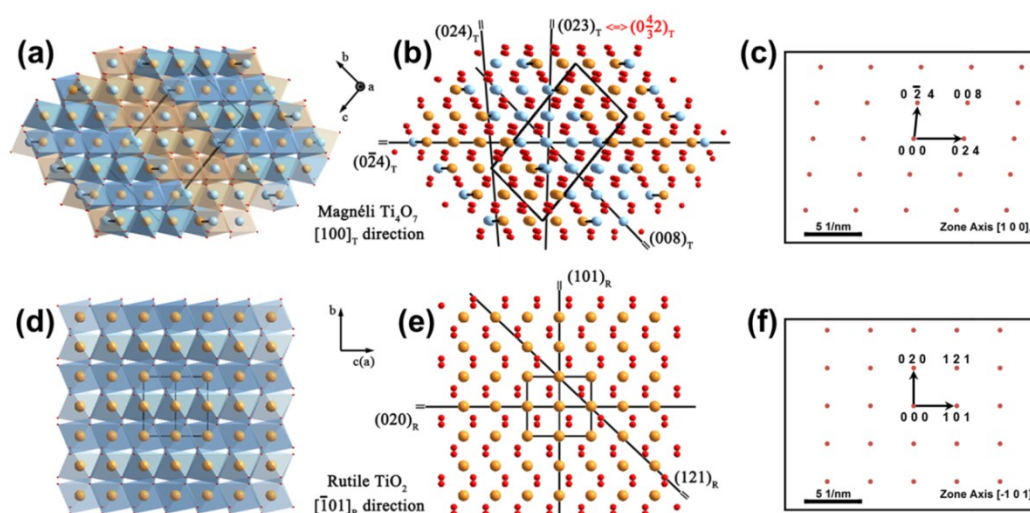


**Figure S5** The structure models for (a)  $\text{Ti}_4\text{O}_7$  at  $[1\ 0\ 0]_T$  and (d) rutile  $\text{TiO}_2$  at  $[\bar{1}\ 0\ 1]_R$ . The typical planes were marked with lines in (b) and (e). Despite the different structure after slipping, there were still some connections between  $\text{Ti}_4\text{O}_7$  and rutile  $\text{TiO}_2$ , such as  $(0\ \bar{2}\ 4)_T$  to  $(0\ 2\ 0)_R$ ,  $(0\ 2\ 4)_T$  and  $(0\ 2\ 3)_T$  to  $(1\ 0\ 1)_R$ . The theoretical diffraction points calculated with the given models indicated a slight change in the angle of base vectors when oxidizing  $\text{Ti}_4\text{O}_7$  to rutile  $\text{TiO}_2$ .

**Table S2** The information of d-spacing and angle for the base vectors. The superscript star (\*) means the diffraction of these planes were weak in XRD results, due to the lattice extinction. The superscript (a) means the data were collected from PDF cards, PDF#50-0787 for  $\text{Ti}_4\text{O}_7$  and PDF#21-

1276 for rutile TiO<sub>2</sub>. The superscript (b) means the data were calculated theoretically using the structural models, icsd#6098 for Ti<sub>4</sub>O<sub>7</sub>, icsd#88625 for rutile TiO<sub>2</sub>.

	Magneli Ti <sub>4</sub> O <sub>7</sub>			Rutile TiO <sub>2</sub>			
	plane index	<i>d</i> -spacing	Angle <V <sub>1</sub> ,V <sub>2</sub> >	plane index	<i>d</i> -spacing	Angle <V <sub>1</sub> ,V <sub>2</sub> >	
vector 1	(0 $\bar{2}$ 4) <sub>T</sub>	2.421 Å <sup>(a)(b)</sup>	—	⇔	(0 2 0) <sub>R</sub>	2.297 Å <sup>(a)(b)</sup>	—
	(0 2 4) <sub>T</sub>	2.137 Å <sup>(a)(b)</sup>	85.15 ° <sup>(b)</sup>				
vector 2	(0 2 3) <sub>T</sub> <sup>*</sup>	2.4494 Å <sup>(b)</sup>	92.38 ° <sup>(b)</sup>	⇔	(1 0 1) <sub>R</sub>	2.487 Å <sup>(a)(b)</sup>	90 ° <sup>(b)</sup>
	(0 1 3) <sub>T</sub> <sup>*</sup>	3.320 Å <sup>(a)(b)</sup>	104.46 ° <sup>(b)</sup>				

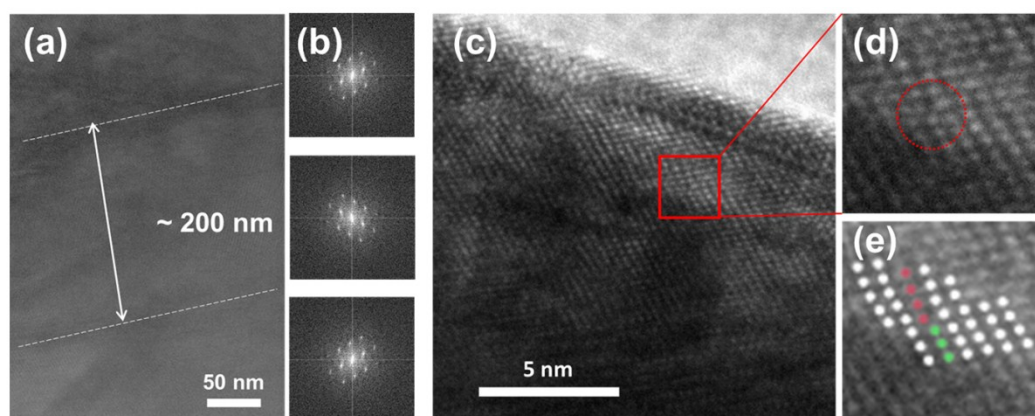


**Figure S6** TEM of the planar defects in the products (15 mol% KClO<sub>4</sub>). (a) The twin crystal was observed. (b) The FFT results of the three regions divided by two twin planes was given. (c) The dislocation of the crystal plane was indicated by the red square. (d) An enlarged figure of the indicated position. (e) The wrong plane is marked with different colors.

**Table S3** The loss of oxygen in products TiO<sub>2-x</sub> was calculated with TG results, which was based on O/Ti ratio in TiO<sub>2</sub>. According to the reaction formula:  $TiO_{2-x} + x [O] \triangleq TiO_2$ , the subscript *x* can be calculated by the mass changes. Considering the residual water in products, which were freeze dried, it was inappropriate to use the initial mass of products (*m*<sub>0</sub>). As shown in Figure S5, the TG curves were all bounded. The maximum mass (*m*<sub>max</sub>) and minimum mass (*m*<sub>min</sub>) of products were the finish and start point of the oxidation process.

samples	test mass	<i>m</i> <sub>0</sub>	<i>m</i> <sub>min</sub> (mg)	<i>m</i> <sub>max</sub> (mg)	<i>m</i> [O] (mg)	<i>m</i> [TiO <sub>2</sub> ] (mg)	<i>x</i>	2- <i>x</i>
Ti <sub>4</sub> O <sub>7</sub>		0	-0.00284	0.54600	0.54884	10.54600	0.260	1.740
15.0 mol%	10 mg	0	-0.07094	0.11219	0.18313	10.11219	0.091	1.909
17.5 mol%		0	-0.05562	0.08403	0.13965	10.08403	0.069	1.931

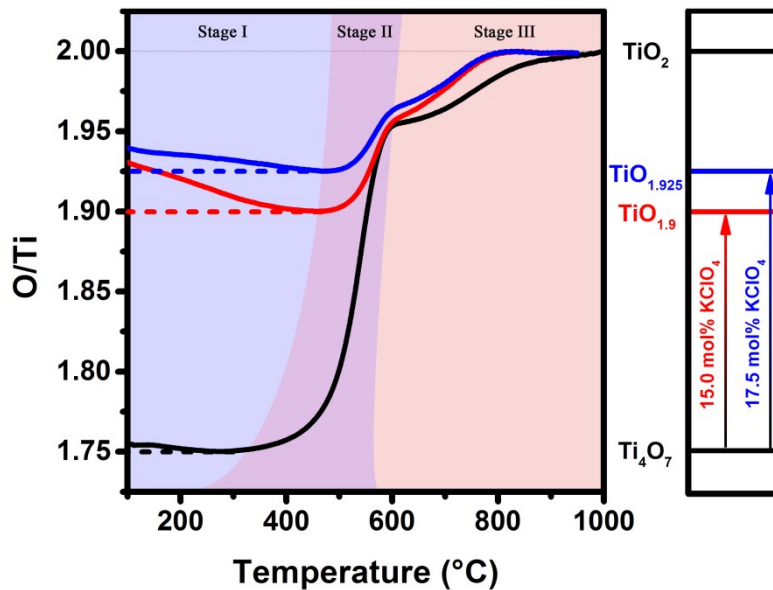


**Figure S7** The TG results of the products, which can be divided into three stages. In stage I, the weight of products decreased due to the loss of residual water. The products denoted as  $\text{TiO}_{1.9}$  and  $\text{TiO}_{1.925}$  were washed by DI water then freeze dried to reduce the KCl. In stage II, the main oxidation process happened when heated at air atmosphere. In stage III, the rate of oxidation was slowed down because the diffusion and redistribution of oxygen between inner and outer layer. Doping amount of  $\text{KClO}_4$  indeed determined the O/Ti ratio in products. Comparing to  $\text{Ti}_4\text{O}_7$ , the oxidation rates of products were much smaller and it was much earlier for the products in this work to finish the oxidation reaction.

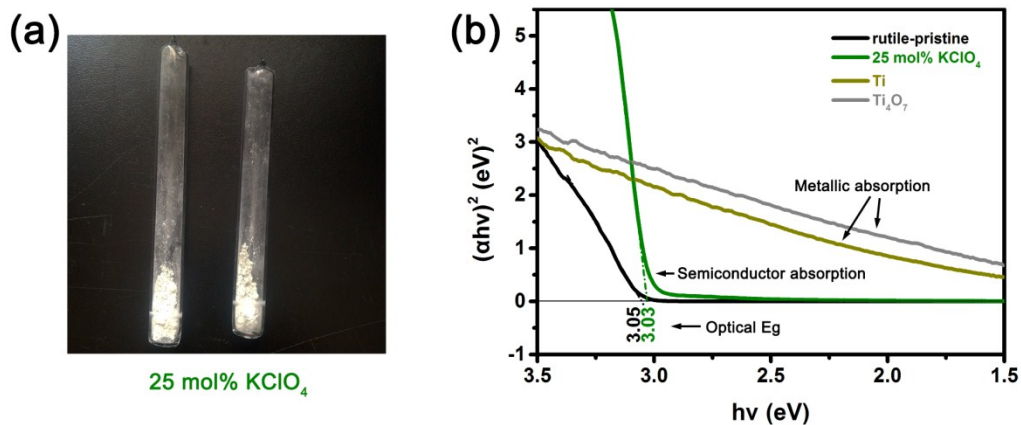


**Figure S8** (a) Digital photo of the supplementary experiments, in which  $\text{Ti}_4\text{O}_7$  was designed to be totally oxidized (the mixing ratio of  $\text{KClO}_4$  is 25 mol%). (b) The calculated  $E_g$  results. The 25 mol% sample exhibits semiconductor absorption, whose  $E_g$  is about 3.03 eV. Ti powder and  $\text{Ti}_4\text{O}_7$  powder have the similar absorption curves, showing metallic absorption.

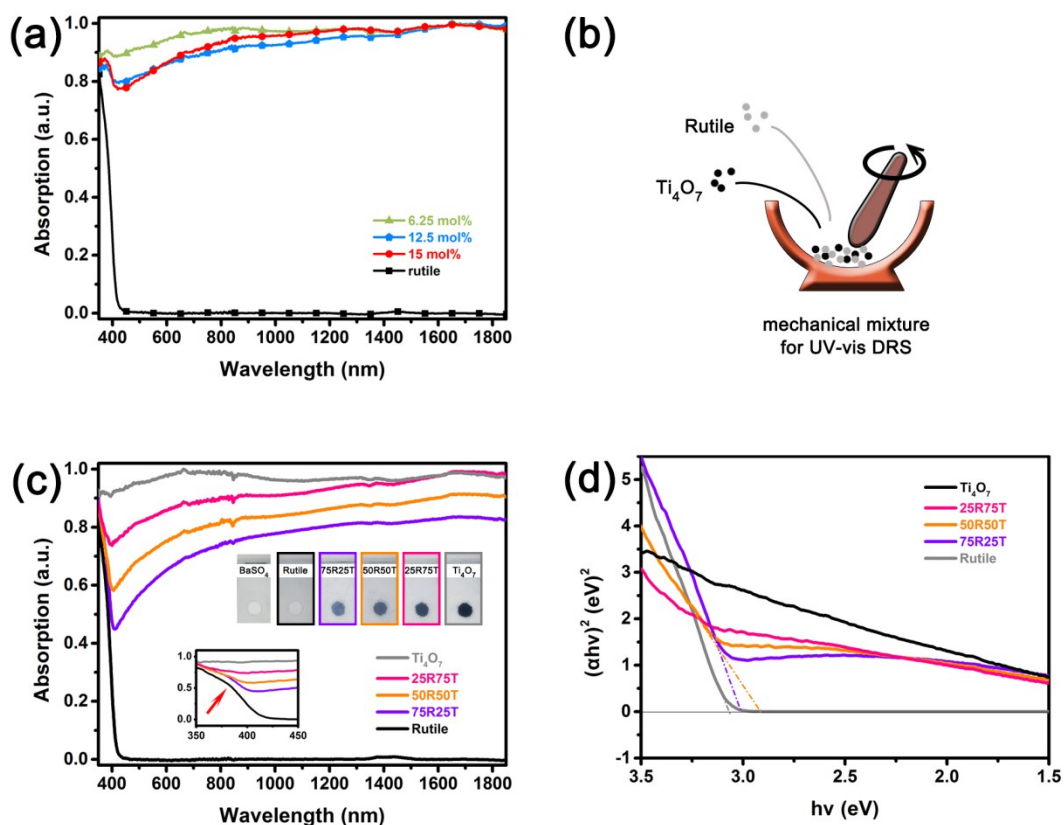


**Figure S9** (a) UV-visible diffuse reflection spectrum (DRS) of the as-prepared mixed phase products. With the mixing ratio of  $\text{KClO}_4$  decreases, the shapes of absorption curves are gradually close to  $\text{Ti}_4\text{O}_7$ , with a metallic absorption characteristic. (b) It urges to be proved that the absorption of mixtures is an overall effect, so raw materials with different mass ratios have been mechanically mixed. (c) UV-vis DRS of the mixtures, in which 25R75T means the mixture of 25 wt% rutile  $\text{TiO}_2$  and 75 wt% Magnéli  $\text{Ti}_4\text{O}_7$ . The colors change and the absorption edges shift. (d) The calculated optical  $E_g$  should be an overall effect, as the only variable is the mixing ratio here.

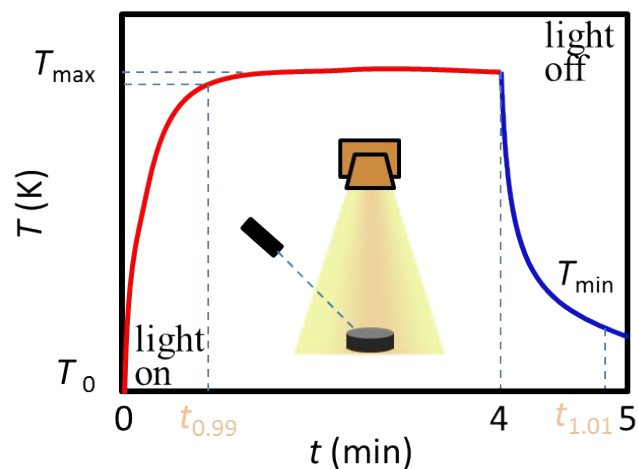


**Figure S10** General photo-thermal response curve obtained in this work. 0.05 g samples were pressed into 8 mm discs under 5 MPa. The temperature of the tested disc was monitored by an IR

sensor. In this experiment, the temperature data were collected when the Xenon lamp simulation was turned on for 4 min then turned off for 1 min. 400 nm cut-off filter was used to test the photo-thermal response of materials outside the UV region. The disc temperature rapidly increased (or decreased) and then stabilized when the light was turned on (or off). The maximum (or minimum) of equilibrium temperature after stabilization can be used to measure the ability of materials to convert light into heat energy under the above test conditions, which is denoted as  $T_{\max}$  (or  $T_{\min}$ ). When the light is on, the time to reach the equilibrium state can partly indicate the speed at which the material converts photo energy into thermal energy. For comparative purposes, the time to reach  $0.99T_{\max}$  was denoted as  $t_{0.99}$ .

1. S. Andersson, A. Sundholm, A. Magnéli, B. Högberg and H. Palmstierna, *Acta Chem. Scand.*, 1959, **13**, 989-997.
2. M. Marezio and P. D. Dernier, *J. Solid State Chem.*, 1971, **3**, 340-348.